Large-Eddy Simulations of realistic atmospheric turbulence with the DLR-TAU-code initialised by in-situ airborne measurements

Torsten Auerswald and Jens Bange

Institute for Geoscience, Universität Tübingen, Germany

Abstract

In this paper the numerical simulation of a turbulent flow in the atmospheric boundary layer (ABL) with an Large-Eddy Simulation (LES)-model is discussed. The results of this work are intended to be used for the numerical simulation of turbulent flows around an airfoil. To simulate the characteristics of the ABL flow and its influence on the airfoil realistically the flow upstream of the airfoil has to be turbulent with statistical properties that are comparable to those found in atmospheric measurements.

To achieve this goal, a method to generate synthetic turbulent wind fields was used to initialise a LES model which is able to simulate the turbulent flow around an airfoil.

For the initial turbulent wind field to contain realistic statistics of atmospheric turbulence data taken with the Helipod system were used. The Helipod is a helicopter-borne measurement probe that is able to take high-resolution measurements of e.g. temperature, wind vector and humidity. The statistical properties that are used as input parameters for the turbulence generator are spectral energy, correlation matrix and the variances of the three components of the wind vector.

The LES model that was used in this project is the flow solver TAU developed by the German Aerospace Center (DLR). TAU is a compressible computational fluid dynamics (CFD) tool that is able to compute the flow around obstacles (e.g. parts of aircrafts or even whole aircrafts) on an unstructured grid. Calculations with TAU can be performed in Reynolds-Averaged Navier-Stokes (RANS)-, LES- or Detached Eddy Simulation (DES)-mode using different sub-grid scale (SGS) models.

1   Introduction

When simulating the flow around obstacles (e.g. airplanes or parts of airplanes) it is very common to perform these simulations on unstructured grids (Mavriplis, 1997). These grids consist of an irregular pattern of geometrical shapes, e.g. tetrahedra, that is fitted to the shape of the obstacle around which the flow is simulated. The grid usually gets finer towards the obstacle. In particular when small radii of curvature occur a very high resolution is needed to represent the shape of the obstacle on the grid properly (see e.g. Rakowitz *et al.*, 2003, for simulations

of the flow around a wing-body configuration on an unstructured grid). In meteorological simulations of the atmospheric boundary layer (ABL), however, much coarser structured grids are used which allow for the coverage of a much larger domain. These simulations are performed from the surface up to an altitude of several kilometers for an area of several square kilometers with a grid spacing of a few ten meters (e.g. Gryschka *et al.*, 2008).

The main interest of the work in this paper is to be able to simulate the interaction of the ABL with an airfoil. The problem occurring here is that the simulation of the flow around the airfoil alone needs too much resources for today's computers to perform a simulation of the whole ABL at the same time. To circumvent this problem the full ABL is not simulated. Instead only a small volume of the actual ABL is simulated within the computational fluid dynamics (CFD)-model. To be able to simulate the ABL flow nevertheless a realistic 3D initial wind field is calculated. For the generation of this wind field statistical properties of measured data are taken as input for a synthetic turbulence generator. These statistical properties are the energy spectrum, the correlation tensor and the variances of wind speed. Even though this is, of course, not a complete representation of the statistics of the flow, some very important properties are considered. The resulting wind field is then used for the initialisation of the CFD-simulation in which the flow around the airfoil is simulated. By using this method it is possible to simulate a turbulent flow and its influence on an airfoil at numerical costs that take into account the limitations of toady's computers.

For the generation of the synthetic turbulent wind field a method is chosen that is based on the Fourier approach where several waves with different wavenumbers are combined to build a random velocity field. This approach was used in earlier works by i.e. Kraichnan (1970) or Fung and Vassilicos (1998). The resulting velocity field is isotropic, gaussian and reproduces a given energy spectrum. It can be modified by applying the method by Lund *et al.* (1998) to obtain a given anisotropic correlation matrix. Another work by Rosales and Meneveau (2006) provides an algorithm to yield realistic non-gaussian statistics while conserving the isotropy and energy spectrum of the velocity field.

2   Method

2.1   Modelling Strategy

The turbulent flow around the airfoil is simulated using the numerical flow solver TAU which was developed by the German Aerospace Center (DLR). Fig. 1 shows a sketch of the model domain. The simulations are performed on two three dimensional grids. The primary grid is a body-fitted unstructured grid around the airfoil. The secondary grid is a cartesian grid upstream of the airfoil on which the turbulent wind field is simulated. During the simulation the secondary grid is advected towards the airfoil using the Chimera technique (see e.g. Schwamborn *et al.*, 2006). In a short distance in front of the airfoil the secondary grid is stopped. Through the right boundary plane the turbulent flow is passed to the primary grid where it can interact with the airfoil. For the simulation of the turbulent wind field on the cartesian grid, TAU is used in LES-mode, while the simulation of the flow around the airfoil is performed in unsteady Reynolds-averaged Navier-Stokes (URANS) mode.
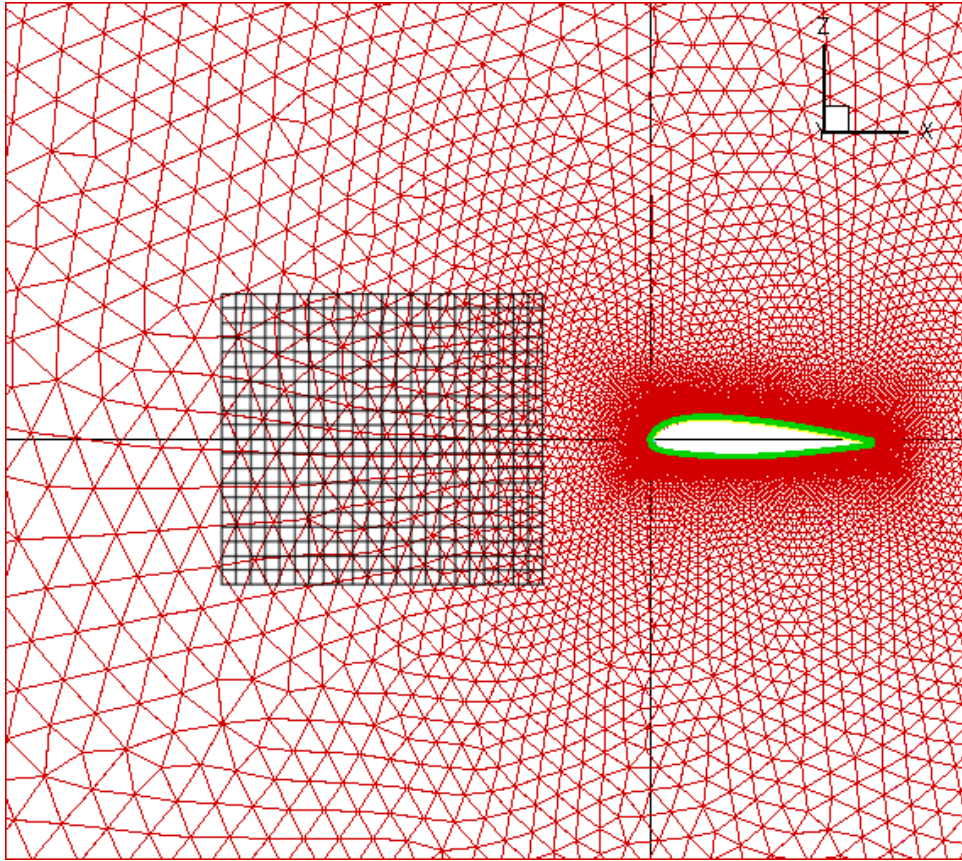
Figure 1: *Sketch of the model domain for the Chimera simulations with TAU. The domain consists of two grids. The primary grid (red) is body-fitted around the airfoil. The secondary cartesian grid (red) is used to simulate the turbulent flow in front of the airfoil.*

2.2   Using input data from measurements

Since the earth surface is not contained in the model domain, there is no driving mechanism for the growth of the atmospheric boundary layer. Therefore, TAU needs to be initialised with an already turbulent flow. For the initial turbulent field to represent realistic weather scenarios measurement data from the Helipod (Bange *et al.*, 2007) is used. The Helipod is an airborne measurement probe which is attached to a helicopter. It was operated on several campaigns taking measurements in the ABL over land surface and the Arctic sea. Measurements were taken at altitudes between 40 m and 2000 m. Several sensors (e.g. wind vector, temperature, humidity) with a resolution of about 100 Hz (corresponding to about 40 m) are mounted for high-resolution measurements in the atmospheric boundary layer. A large data set of measurements for different meteorological scenarios is available including atmospheric flow in various thermal stratifications (stable, very stable, neutral, convective).

2.3   Generating the synthetic turbulent wind field

The problem that occurs when using the Helipod measurements as initialisation for TAU is that the dataset is only one dimensional whereas the TAU domain is three dimensional. Therefore, the measured data can not be used directly. Rather the statistics of the data is calculated and

a synthetic three-dimensional turbulent wind field is generated possessing the same statistical properties as the measurements. The input statistics for the turbulence generator are the energy spectrum, the correlation matrix and the variances of the wind vector components. Using these statistics the velocity field is generated by calculating a Fourier series. In Fourier space several spectral velocity vectors are combined to build a turbulent vector field in position space. The basic equation is written as follows:

$$\vec{v}(\vec{x}) = \sum_{n=1}^{N} \sum_{m=1}^{N} \sum_{l=1}^{N} \left(\vec{C}_{n,m,l} \big(\cos(\vec{k}_{n,m,l} \cdot \vec{x}) + i \sin(\vec{k}_{n,m,l} \cdot \vec{x}) \big) \right), \tag{1}$$

where $\vec{v}$ is the velocity vector, $\vec{x}$ is the position vector, N is the total number of wavenumbers in every direction of the wavenumber space (due to the Nyquist-Theorem N should be chosen half the number of grid points M in one direction), $\vec{k}_{n,m,l}$ are the wavenumber vectors and $\vec{C}_{n,m,l}$ the complex amplitude vectors.

The amplitude vectors represent the spectral velocities for the corresponding wavenumber. The absolute values of these vectors are calculated from $E(|\vec{k}_{n,m,l}|)$, the spectral energy per wavenumber interval $\Delta|\vec{k}_{n,m,l}|$, which, e.g., can be calculated from the measured timeseries:

$$|\vec{C}_{n,m,l}| = \sqrt{\frac{1}{Z_{n,m,l}} \cdot E(|\vec{k}_{n,m,l}|) \cdot \Delta|\vec{k}_{n,m,l}|}, \tag{2}$$

where $Z_{n,m,l}$ is the number of occurrence of the same absolute values of $\vec{k}_{n,m,l}$ for all given combinations of n, m and l. In case of an energy spectrum calculated from measurements, the random fluctuations of that energy spectrum contribute an additional random effect to the synthetic wind field.

Often, turbulent velocity fields are simulated with compressible flow solvers. In these cases the divergence of the velocity field plays an important role. If the divergence of the velocity field is non-zero, density fluctuations appear in the domain which propagate with the speed of sound. Since sound waves can often not be resolved by the model (because the grid spacing or timestep is not small enough) this can lead to massive errors or model crashes. Therefore, it is an important feature for the random flow generator to produce divergence-free velocity fields. Taking the divergence of the velocity field in eq.1 yields:

$$\nabla \cdot \vec{v}(\vec{x}) = \sum_{n=1}^{N} \sum_{m=1}^{N} \sum_{l=1}^{N} \left(\vec{C}_{n,m,l} \cdot \vec{k}_{n,m,l} \big(i \cos(\vec{k}_{n,m,l} \cdot \vec{x}) - \sin(\vec{k}_{n,m,l} \cdot \vec{x}) \big) \right). \tag{3}$$

The divergence of the generated velocity field is zero if the scalar product $\vec{C}_{n,m,l} \cdot \vec{k}_{n,m,l}$ is zero, which is the case when $\vec{C}_{n,m,l}$ and $\vec{k}_{n,m,l}$ are perpendicular. In Kraichnan (1970), e.g., this is achieved by calculating random auxiliary vectors $\vec{f}_{n,m,l}$ that are equally distributed on the unit sphere:

$$\vec{f}_{n,m,l} = (\sin\theta_{n,m,l} \cos\phi_{n,m,l}, \sin\theta_{n,m,l} \sin\phi_{n,m,l}, \cos\theta_{n,m,l}), \tag{4}$$

with $\theta_{n,m,l}$ and $\phi_{n,m,l}$ being spherical coordinates for the unit sphere which are chosen randomly. For each wavenumber the vector product of the random auxiliary vector $\vec{f}_{n,m,l}$ and the unit vector of the wavenumber is calculated. The resulting unit vectors are equally distributed on the unit sphere and are perpendicular to the wavenumber vectors:

$$\vec{e}_{\vec{c}_{n,m,l}} = \frac{1}{|\vec{f}_{n,m,l} \times \vec{e}_{\vec{k}_{n,m,l}}|} \vec{f}_{n,m,l} \times \vec{e}_{\vec{k}_{n,m,l}}. \tag{5}$$

By applying the above equations a synthetic turbulent wind field is generated which contains isotropic turbulence with a prescribed energy spectrum $E(|\vec{k}_{n,m,l}|)$. Prescribed variances can be reproduced by scaling the velocity components:

$$v_{i_{n,m,l}} = v_{i_{n,m,l}}^{\text{gen}} \frac{\sqrt{\sigma_i^{\text{data}}}}{\sqrt{\sigma_i^{\text{gen}}}}, \tag{6}$$

with $i = 1..3$ denoting the three components of the wind vector, $v_{i_{n,m,l}}^{\text{gen}}$ being the i-th component of the velocity field generated by the turbulence generator, σ_i^{gen} being the variance of the i-th component of the generated velocity field and σ_i^{data} being the variance of the i-th component of the measured velocity time series.

2.4 Modification for anisotropic turbulence

By using the method of Lund *et al.* (1998) it is possible to produce turbulent wind fields with given anisotropic statistics. The anisotropic wind field is constructed by applying a transformation tensor to the isotropic wind field:

$$v_{i_{n,m,l}}^{\text{aniso}} = a_{ij} \cdot v_{j_{n,m,l}}^{\text{iso}}. \tag{7}$$

The transformation tensor a is defined as:

$$a = \begin{pmatrix} \sqrt{R_{11}} & 0 & 0 \\ R_{21}/a_{11} & \sqrt{R_{22} - a_{21}^2} & 0 \\ R_{31}/a_{11} & (R_{32} - a_{21}a_{31})/a_{22} & \sqrt{R_{33} - a_{31}^2 - a_{32}^2} \end{pmatrix}, \tag{8}$$

where **R** is the given correlation tensor, e.g. calculated from measurements, that is imposed on the velocity field. The correlations of the resulting velocity field $v_{i_{n,m,l}}^{\text{aniso}}$ are equal to R_{ij}.

2.5 Calculation of the density and pressure field

The turbulence generator only delivers a turbulent wind field, therefore an initial density and pressure field has to be calculated to start a TAU simulation. Since TAU is a compressible flow solver the simulation is very sensitive to the initial field. A good guess for the density and pressure field can be made by applying the Bernoulli equation which gives a relation between wind speed and density or pressure, respectively. The equations are:

$$p = p_\infty \left(1 + \frac{\gamma - 1}{2} i \text{Ma}^2 \right)^{\frac{\gamma}{1-\gamma}}, \tag{9}$$

$$\rho = \rho_\infty \left(1 + \frac{\gamma - 1}{2} \text{Ma}^2 \right)^{\frac{1}{1-\gamma}}, \tag{10}$$

with p_∞ and ρ_∞ being the reference values for pressure and density, γ the adiabatic coefficient and Ma the Mach number.
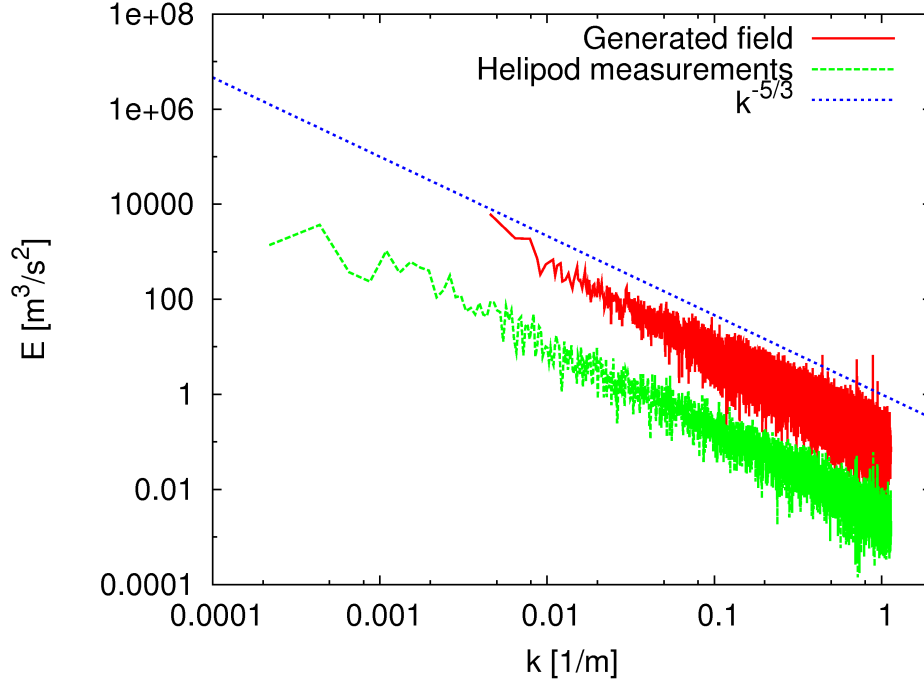
Figure 2: *Energy spectrum of the generated synthetic wind field (red line) and the spectrum of the Helipod measurements (green, dashed) that was used as input for the turbulence generator. The spectrum of the synthetic wind field is multiplied by factor 50 for better visibility of the two spectra. For comparison the $k^{-5/3}$ slope is plotted (blue, dotted).*

3 Results

3.1 The synthetic wind field

A turbulent wind field was generated using the turbulence generator presented in section 2.3. The input statistics for the turbulence generator were calculated from measurements from the LITFASS 2003 campaign (Bange *et al.*, 2006) which was conducted in the north-east of Germany in Lindenberg near Berlin from May, 24th, to June, 17th. The aim of this campaign was to measure turbulent fluxes over heterogeneous terrain in a convective boundary layer. For the generation of the synthetic turbulent wind field measurements from June, 2nd, were chosen. The spectrum calculated from these measurements is shown in fig. 2 (green, dashed). It shows the $k^{-5/3}$ slope of the inertial subrange of locally isotropic turbulence (Kolmogorov, 1941) over the whole wavenumber range. The spectrum from the synthetic wind field (red line in fig. 2) matches the input spectrum from the Helipod measurements very well (it was multiplied by a factor of 50 for better visibility). It is obvious that it can not cover the large scales from the measurements since the model domain has a size of only 350 m (500 points in each direction, grid spacing of 0.7 m) while the Helipod flight leg had a length of about 4600 m .

The synthetic wind field was modified to obtain the anisotropic wind correlations from the measurement data. The correlation matrices from the measurement data and from the synthetic wind field as shown in table 1 are in good agreement as well as the variances which, due to the scaling of the wind field (eq. 6), match the given variances perfectly.

Helipod measurements				Generated field			
	u	v	w		u	v	w
u	1	0.087	0.119	u	1	0.079	0.097
v	0.087	1	-0.004	v	0.079	1	-0.005
w	0.119	-0.004	1	w	0.097	-0.005	1

Table 1: *Correlation matrices calculated from the Helipod measurements (left) and the synthetic wind field (right).*
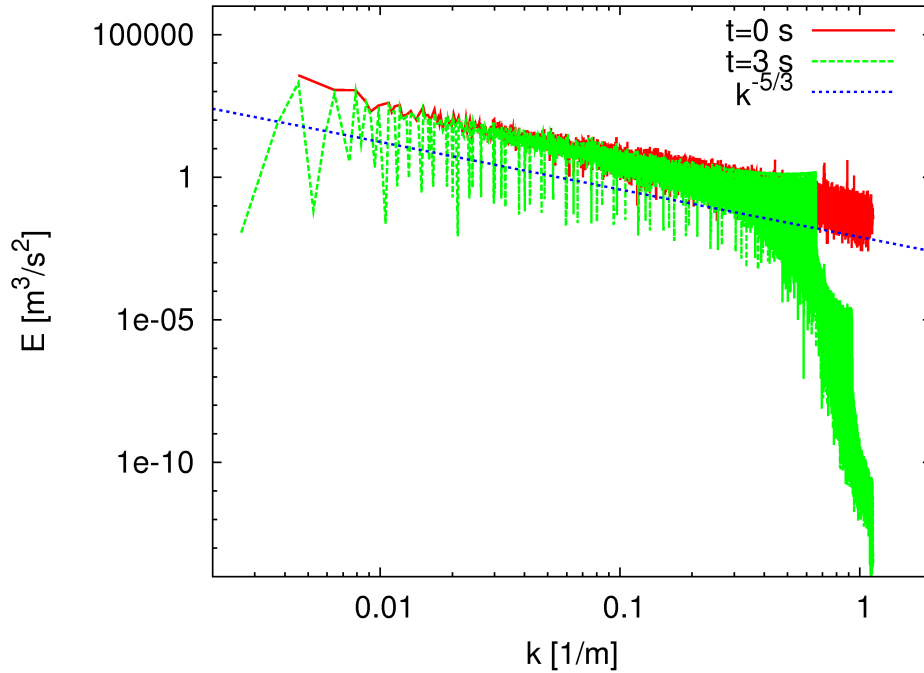

Figure 3: *Energy spectra of the simulations with TAU. Depicted is the spectrum of the initial wind field (red line) and after 3 seconds simulation time (green, dashed). For comparison the $k^{-5/3}$ slope is plotted (blue, dotted).*

3.2 TAU simulations

Using the results presented in section 3.1 it is now possible to initialise the TAU model with a three-dimensional turbulent wind field that possesses important statistical properties of a real (since measured) ABL flow. In order to make sure TAU gives good results for the simulation of the turbulent wind field the model is run in LES mode first. In these simulations only the secondary grid (cp. fig. 1) is considered.

Fig. 3 compares the energy spectrum of the initial wind field with the spectrum after three seconds of simulation time. There is a massive loss of energy in the small scales between about 0.3 m^{-1} and 1.2 m^{-1} due to numerical dissipation. This affects eddies of the size of $1 \cdot \Delta x$ to about $4 \cdot \Delta x$ (δx being the grid spacing). The loss of these turbulent scales is the common behaviour of LES-models and was expected. Scales larger than $4 \cdot \Delta x$ are preserved very well. The energy spectrum after 3 seconds is shifted marginally to lower energy and follows in average the $k^{-5/3}$ slope nearly over the entire wavenumber range.

In table 2 it can be seen that the correlations of the velocity components change significantly. The variances of the velocity components decrease since turbulent energy is dissipated with

	Initial field				After 3 s		
	u	v	w		u	v	w
u	1	0.079	0.097	u	1	-0.002	0.057
v	0.079	1	-0.005	v	-0.002	1	-0.182
w	0.097	-0.005	1	w	0.057	-0.182	1

$\sigma_u = 2.24 \text{ m}^2/\text{s}^2$ $\sigma_u^2 = 1.84 \; m^2/s^2$

$\sigma_v = 2.73 \text{ m}^2/\text{s}^2$ $\sigma_v^2 = 1.90 \; m^2/s^2$

$\sigma_w = 1.16 \text{ m}^2/\text{s}^2$ $\sigma_w^2 = 1.01 \; m^2/s^2$

Table 2: *Correlation matrices and variances of the velocity components as calculated from the TAU simulations at $t = 0$ s (left) and $t = 3$ s (right).*
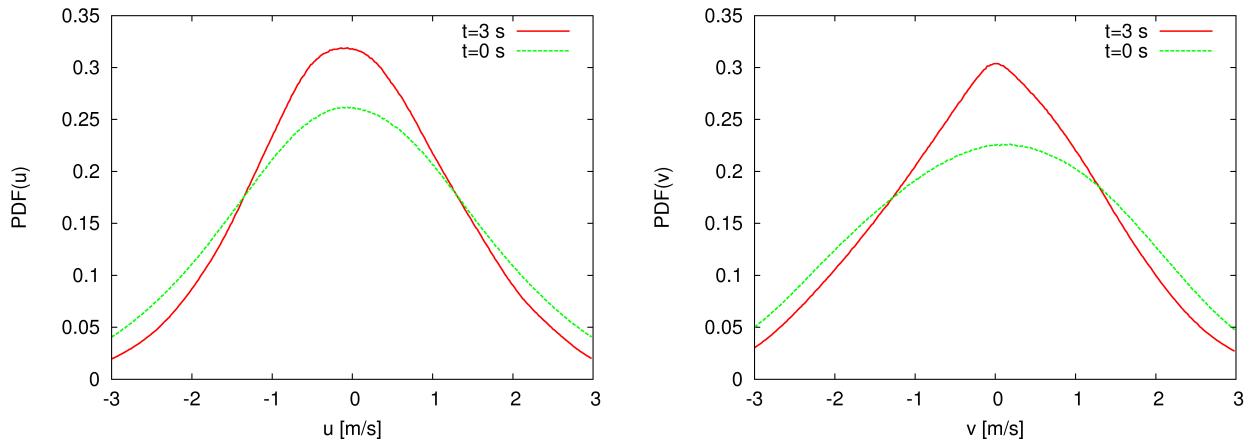

Figure 4: *Probability density function calculated from the x-component (left) and y-component (right) of the velocity in the initial wind field (green, dashed) and the TAU result after 3 s of simulation (red line).*

time. This effect is also noticeable in the plots of the probability density functions (PDF's) of the velocity components (fig. 4 and 5) where the density functions become narrower with time since the large velocity values occur less often.

An important feature of the atmospheric boundary layer is the intermittency of the turbulent flow. This effect can be seen in the PDF of the difference of the velocity over a certain separation distance. Due to intermittent fluctuations the PDF of velocity increments deviates from the PDF of the normal distribution by having tails on the left and right end of the function (see e.g. Sreenivasan (1999) for a short summary on intermittency). Fig. 6 (left) shows the PDF of the velocity increments of the initial wind field. For all separation distances the PDF's are Gaussian. After three seconds however, the flow has adapted to a more realistic state (see fig. 6, right) exhibiting significant tails. These tails develop due to sudden bursts occurring in intermittent flows. As a consequence strong events are much more likely than in a Gaussian distribution which is represented by an increase of the PDF at the left and right end of the distribution. Also visible is that, like in real flows, the PDF of the increments of the velocity becomes more Gaussian with larger separation distances. For a separation distance of 32 times the grid spacing the PDF is nearly Gaussian.
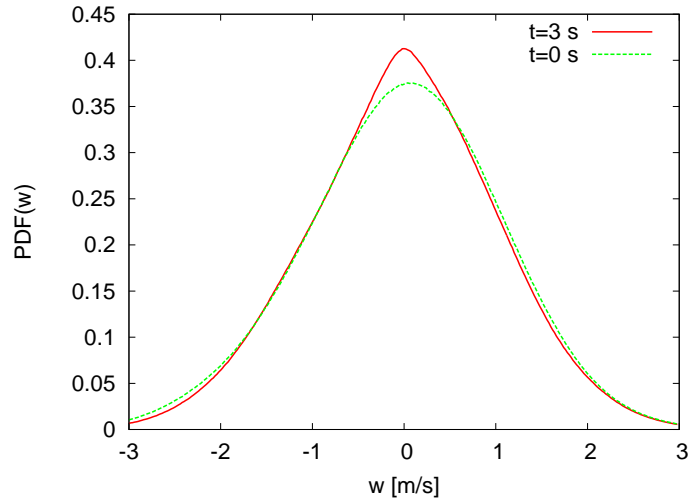
Figure 5: *Probability density function calculated from the z-component of the velocity in the initial wind field (green, dashed) and the TAU result after 3 s of simulation (red line).*
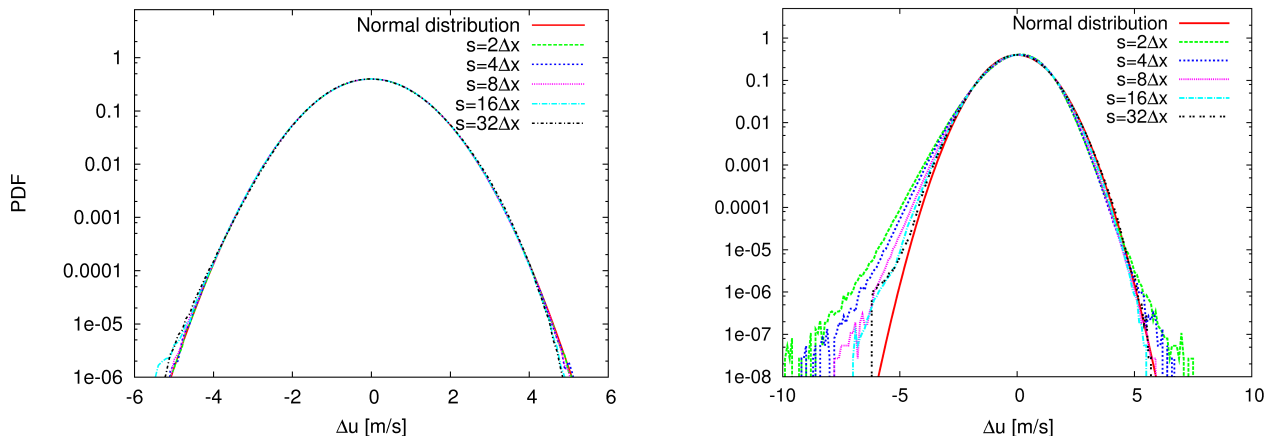

Figure 6: *Normalised PDF of the increments of the x-component of the velocity calculated from the initial wind field (left) and the TAU result after 3 s (right) for separation distances s=1.4 m (green), s=2.8 m (blue), s=5.6 m (purple),s=11.2 m (light blue) and s=22.4 m (black). For comparison the PDF of the normal distribution is plotted in red.*

4   Conclusion

This projects aims at simulating the interaction of a turbulent flow with an airfoil and thereby simulating conditions an airfoil would meet when flying through the atmospheric boundary layer. For this purpose a realistic atmospheric flow has to be established in the model domain. It was shown that by using the method in section 2.3 it is possible to generate synthetic turbulent wind fields possessing some important features of realistic atmospheric turbulence. In section 3.2 first results from simulations with the CFD solver TAU were presented showing the general ability to initialise TAU with the generated wind fields. The results show that the key features of the flow are well preserved within a 3 s-simulation (beside the correlation matrix which showed some major deviations) and in addition develops realistic PDF's of the velocity increments during the simulation. Therefore, it can be concluded that this method of simulating turbulent flows is well suited for further simulations on a Chimera grid where the generated turbulent flow can actually interact with an airfoil.

Acknowledgments

References

Bange, J., **Spieß, T.**, **Herold, M.**, **Beyrich, F.** and **Hennemuth, B.**, **2006**: Turbulent Fluxes from Helipod Flights above Quasi-Homogeneous Patches within the LITFASS Area. *Boundary-Layer Meteorol.*, **121**, 127–151.

Bange, J., **Spieß, T.** and **van den Kroonenberg, A.**, **2007**: Characteristics of the Early-Morning Shallow Convective Boundary Layer from Helipod Flights during STINHO-2. *Theor. Appl. Climatol.*, **90**, 113–126.

Fung, J. C. H. and **Vassilicos, J. C.**, **1998**: Two-particle dispersion in turbulentlike flows. *Physical Reviews E*, **57**, 1677–1690.

Gryschka, M., **Drüe, C.**, **Etling, D.** and **Raasch, S.**, **2008**: On the influence of sea-ice inhomogeneities onto roll convection in cold-air outbreaks. *Geophys. Res. Lett.*, **35**.

Kolmogorov, A. N., **1941**: Energy dissipation in locally isotropic turbulence. *Doklady AN SSSR*, **32**, 19–21.

Kraichnan, R. H., **1970**: Diffusion by a Random Velocity Field. *The Physics of Fluids*, **13**, 22–31.

Lund, T. S., **Wu, X.** and **Squires, K. D.**, **1998**: Generation of Turbulent Inflow Data for Spatially-Developing Boundary Layer Simulations. *J. Comput. Phys.*, **140**, 233–258.

Mavriplis, D. J., **1997**: Unstructured Grid Techniques. *Ann. Rev. of Fluid Mechanics*, **29**, 473–514.

Rakowitz, M., **B.Eisfeld**, **Schwamborn, D.** and **Sutcliffe, M.**, **2003**: Structured and Unstructured Computations on the DLR-F4 Wing-Body Configuration. *J. of Aircraft*, **40**, 256–264.

Rosales, C. and **Meneveau, C.**, **2006**: A minimal multiscale Lagrangian map aproach to synthesize non-Gaussian turbulent vector fields. *Physics of Fluids*, **18**.

Schwamborn, D., **Gerhold, T.** and **Heinrich, R.**, **2006**: The DLR TAU-Code: Recent Applications in Research and Industry. *ECCOMAS CFD 2006*.

Sreenivasan, K. R., **1999**: Fluid turbulence. *Rev. Modern Phys.*, **71**, 383–395.